Mech. Sci., 17, 545–555, 2026
https://doi.org/10.5194/ms-17-545-2026

Mechanical Sciences
Open Access

Effect of engine torque fluctuations under different flight conditions on the torsional vibration response of helicopter power input chain

Hongli Yue[1], Chao Li[1], Guangfu Bin[1], Xianghuan Liu[2], Jian Li[3], Anhua Chen[1], and Qiang Li[1]

[1]School of Mechanical Engineering, Hunan University of Science and Technology, Xiangtan, 411201, China
[2]Hunan Key Laboratory of New Energy Power and Transmission System, Zhuzhou Gear Co., Ltd., Zhuzhou, 412000, China
[3]AECC HAPRI Aviation Key Laboratory of Aero-engine Vibration Technology, Zhuzhou, 412002, China

Correspondence: Chao Li (lichao911016@126.com)

Received: 20 March 2026 – Revised: 8 April 2026 – Accepted: 27 April 2026 – Published: 20 May 2026

Abstract. Under varying flight conditions, helicopter turboshaft engines generate pronounced torque fluctuations that can intensify torsional vibration in the power input chain, accelerating fatigue damage of critical transmission components and threatening flight safety. A lumped-parameter coupled dynamic model of the power turbine and power input chain is developed with time-varying torque excitation. Measured torque signals from three representative flight conditions – hover, high-altitude climb and descent maneuver, and aggressive vertical maneuvers – are applied as inputs to compare torsional responses. Results show that the torque variation rate dominates vibration intensity, as rapid changes promote transient energy accumulation and inertia mismatch within the transmission system. Aggressive vertical maneuvers produce the highest variation rate and the largest torsional response; the torsional angle at the strut-type overrunning clutch is about 10.3 % higher than that in the high-altitude climb and descent maneuver and 280.0 % higher than in hover. These findings clarify the mechanism by which realistic engine torque fluctuations affect torsional vibration and provide theoretical support for the dynamic design and reliability evaluation of helicopter transmission systems.

1 Introduction

In helicopters, the power input chain (PIC) linking the power turbine to the main rotor plays a key role in power transmission efficiency and overall system reliability (de Voogt and St Amour, 2021). Under real operating conditions, engine output torque exhibits pronounced nonstationary and time-varying characteristics due to factors such as gas generator instability, aerodynamic disturbances, and fuel control fluctuations (Vladov et al., 2025; Ma et al., 2024; Song et al., 2025). Severe torque fluctuations can significantly amplify torsional vibrations, inducing alternating stresses that lead to fatigue, reduced component life, and degraded reliability, potentially threatening flight safety (Davies et al., 2013; Han et al., 2015).

Torque fluctuation has been widely recognized as a dominant excitation source in aerospace transmission systems. Recent studies show that nonstationary torque excitation can increase cyclic stresses in shafts and gears, accelerate crack initiation and propagation, and aggravate lubrication degradation in geared drivetrains (Hu et al., 2022, 2025; van Binsbergen et al., 2023). When excitation frequencies approach system natural frequencies, torsional resonance may occur and significantly amplify dynamic responses (Liu et al., 2022). In twin-engine helicopter configurations, torque imbalance can further intensify dynamic loads and fatigue damage in critical drivetrain components (Chi et al., 2019; Lin et al., 2025). These findings highlight the necessity of accurately characterizing torque-induced torsional vibration in helicopter transmission systems.

Extensive research has been devoted to torsional vibration and dynamic characteristics of helicopter gear transmissions. With the rapid development of computational methods, studies have evolved from simplified drivetrain repre-

sentations to high-fidelity coupled dynamic models incorporating rotor–engine–transmission interactions, nonlinear gear meshing, and spline contact effects (Wang and Xia, 2022; Mo et al., 2023; Che et al., 2024; Zhu et al., 2024). In parallel, torsional vibration signals have been widely applied to gear fault diagnosis and health monitoring, demonstrating strong capability in detecting gear damage and tracking fault evolution (Shen et al., 2021; Yang et al., 2023). Recent developments further emphasize multi-physics and transient dynamic modeling of helicopter propulsion systems. High-fidelity turboshaft-engine modeling and hybrid approaches combining finite-element and multibody dynamics have significantly improved understanding of transient load transfer and nonlinear vibration mechanisms in complex drivetrain systems (Sheng et al., 2020; Li et al., 2022).

In summary, most existing studies adopt constant or idealized harmonic torque excitations and mainly investigate rotor dynamic responses under simplified conditions. In real helicopter operations – particularly during high-altitude climb and descent and aggressive vertical maneuvers – the engine output torque exhibits strong nonstationary and time-varying characteristics that deviate markedly from these assumptions. Systematic investigations into the influence of such realistic torque fluctuations on torsional vibration remain limited. To address this gap, a coupled dynamic model of the power turbine and power input chain (PT–PIC) is developed. Using measured torque data from three representative flight conditions – hover, high-altitude climb and descent, and aggressive vertical maneuvers – the effects of torque fluctuations on torsional vibration responses are analyzed, and the underlying mechanisms are clarified from a system-level perspective.

The remainder of this paper is organized as follows. Section 2 presents the PT–PIC dynamic model and characterizes torque excitation. Section 3 provides numerical results and a comparative analysis of system responses under different operating conditions. Finally, Sect. 4 summarizes the main conclusions and outlines future research directions.

2 Dynamic modeling of PT–PIC

This section first presents a mechanistic analysis to clarify the relationship between torque variation rate and the system's transient response, thereby revealing how torque fluctuations influence torsional vibrations. The structural configuration of the PT–PIC is then described, followed by the development of a lumped-parameter torsional dynamic model with torque fluctuation excitation and the derivation of the governing equations of motion. Finally, based on measured engine torque data, the time-domain characteristics under different flight conditions are analyzed. An autocorrelation function is employed to quantify the temporal correlation and variation rate of torque signals, enabling the classification of excitation features and supporting comparative analysis of torsional vibration responses.

2.1 Mechanism of torque fluctuation effects on rotor torsional vibration response

To investigate the influence of engine torque fluctuations on the response amplitude and transient characteristics of the rotor system, this section conducts a theoretical analysis based on a representative single-degree-of-freedom (SDOF) torsional vibration model. From a mechanistic perspective, the intrinsic interaction between torque fluctuations and system dynamic response is elucidated, thereby providing theoretical support for the subsequent analysis of multi-degree-of-freedom (MDOF) systems.

The torsional equation of motion for a typical SDOF system can be expressed as

$$J\ddot{\theta} + c\dot{\theta} + k\theta = T(t), \tag{1}$$

where J denotes the rotational inertia, c the torsional damping coefficient, k the torsional stiffness, and $T(t)$ the external input torque.

Considering that the engine output torque under real operating conditions exhibits pronounced nonstationary fluctuation characteristics, its variation process, although complex, generally possesses a finite rate of change that is much smaller than the theoretically infinite rate associated with an ideal step load. Therefore, within a sufficiently small time interval, the torque fluctuation signal can be approximated in a piecewise manner as a linear function with a time-varying slope, i.e., an equivalent ramp-type torque input: $T(t) = \alpha t$, where α denotes the rate of torque variation.

Applying the Laplace transform to Eq. (1) yields

$$Js^2\Theta(s) + cs\Theta(s) + k\Theta(s) = \frac{\alpha}{s^2}. \tag{2}$$

After obtaining the transfer function, it can be reformulated into the standard second-order system representation, which is expressed as

$$\Theta(s) = \frac{\alpha/J}{s^2\left(s^2 + 2\zeta\omega_n s + \omega_n^2\right)}. \tag{3}$$

Applying the inverse Laplace transform yields the torsional response of the SDOF system as

$$\theta(t) = \frac{\alpha}{k}\left[t - \frac{2\zeta}{\omega_n} + e^{-\zeta\omega_n t}\left(A\cos(\omega_d t) + B\sin(\omega_d t)\right)\right], \tag{4}$$

where $\omega_n = \sqrt{\frac{k}{J}}$ denotes the natural frequency of the system, $\zeta = \frac{c}{2\sqrt{Jk}}$ is the damping ratio, and $\omega_d = \omega_n\sqrt{1-\zeta^2}$ is the damped natural frequency. The constants A and B are determined by the initial conditions.

According to Eq. (4), the system response can be decomposed into three components:

1. *The linear growth term* $\frac{\alpha t}{k}$. This term represents the quasi-static response associated with the time-varying torque input. Its slope is directly proportional to the torque variation rate α.

2. *The constant term*. This term reflects the modulation of the long-term response by the inherent system damping.

3. *The exponentially decaying oscillatory term.* This component corresponds to the transient torsional response induced by the variation in the input excitation. Its amplitude is dependent on the torque variation rate α, while its decay timescale is governed by system damping.

These results indicate that the torque variation rate α is the key parameter controlling transient response intensity. Larger α produces stronger transient vibrations, whereas smaller α leads to rapid attenuation toward a quasi-static state. Overall, torsional vibration is governed primarily by the torque variation rate rather than its amplitude, providing a theoretical basis for analyzing torque fluctuation effects in subsequent MDOF models.

2.2 Dynamic model of the PT–PIC

The PIC, a key component of the transmission system, transfers engine power to the combining gearbox, which drives the main and tail rotors. It comprises the power shaft, first-stage reduction gear pair, elastic shaft, second-stage reduction pinion, and combining gear, interconnected by spline and diaphragm couplings, as well as a strut-type overrunning clutch for engagement control. As the power turbine is directly coupled to the PIC, its torque fluctuations strongly affect the torsional response of the system. The 3D schematic of the PT–PIC system is shown in Fig. 1.

A lumped-parameter approach is adopted to model the PT–PIC system. Each component is represented by rigid disks, massless damping, and torsional elastic elements, considering only torsional degrees of freedom. Nonlinear effects such as gear meshing errors and backlash are neglected to emphasize the dominant influence of torque excitation. The system is thus simplified into an 8-degree-of-freedom torsional model, as shown in Fig. 1, with angular displacements of the equivalent inertia disks as generalized coordinates. Based on this model, the torsional vibration responses under different torque fluctuation excitations can be systematically analyzed.

The rotational inertia of each component is obtained through SolidWorks-based modeling, while the corresponding torsional stiffness values are calculated via finite-element analysis using ANSYS. The resulting parameters of the equivalent disks and the dynamic properties of each component are summarized in Tables 1–2.

Based on Newton's second law, the torsional vibration dynamic equations of the coupled PT–PIC system, incorporating the effects of engine torque fluctuations, are established as follows:

$$\begin{cases} J_1\ddot{\theta}_1 + c_1\left(\dot{\theta}_1 - \dot{\theta}_2\right) + k_1\left(\theta_1 - \theta_2\right) = T_1 \\ J_2\dot{\theta}_2 + c_1\left(\dot{\theta}_2 - \dot{\theta}_1\right) + c_2\left(\dot{\theta}_2 - \dot{\theta}_3\right) + k_1\left(\theta_2 - \theta_1\right) \\ +k_2\left(\theta_2 - \theta_3\right) = 0 \\ J_3\dot{\theta}_3 + c_2\left(\dot{\theta}_3 - \dot{\theta}_2\right) + c_3\left(\dot{\theta}_3 - \dot{\theta}_4\right) + k_2\left(\theta_3 - \theta_2\right) \\ +k_3\left(\theta_3 - \theta_4\right) = 0 \\ J_4\ddot{\theta}_4 + c_3\left(\dot{\theta}_4 - \dot{\theta}_3\right) + k_3\left(\theta_4 - \theta_3\right) + T_{d1}r_{b1} = 0 \\ J_5\ddot{\theta}_5 + c_5\left(\dot{\theta}_5 - \dot{\theta}_6\right) + k_5\left(\theta_5 - \theta_6\right) - T_{d1}r_{b2} = 0 \\ J_6\ddot{\theta}_6 + c_5\left(\dot{\theta}_6 - \dot{\theta}_5\right) + c_6\left(\dot{\theta}_6 - \dot{\theta}_7\right) \\ +k_5\left(\theta_6 - \theta_5\right) + k_6\left(\theta_6 - \theta_7\right) = 0 \\ J_7\ddot{\theta}_7 + c_6\left(\dot{\theta}_7 - \dot{\theta}_6\right) + k_6\left(\theta_7 - \theta_6\right) + T_{d2}r_{b3} = 0 \\ J_8\ddot{\theta}_8 - T_{d2}r_{b4} = -T_2 \\ T_{d1} = c_{m1}\left(r_{b1}\dot{\theta}_4 - r_{b2}\dot{\theta}_5\right) + k_{m1}\left(r_{b1}\theta_4 - r_{b2}\theta_5\right) \\ T_{d2} = c_{m2}\left(r_{b3}\dot{\theta}_7 - r_{b4}\dot{\theta}_8\right) + k_{m2}\left(r_{b3}\theta_7 - r_{b4}\theta_8\right), \end{cases} \tag{5}$$

where T_1 and T_2 denote the power turbine torque and load torque, respectively. For each operating condition, T_2 is assumed constant and determined by multiplying the mean value of the measured T_1 by the overall transmission ratio, representing steady rotor power demand while ensuring that torsional response variations are primarily driven by the time-varying fluctuations of T_1. $\theta_i\,(i = 1, 2, \ldots, 8)$ denotes the torsional displacement of the equivalent disks. Gears 1–2 represent the first-stage reduction pair, and gears 3–4 represent the second-stage reduction pair. $r_{bi}\,(i = 1, 2, 3, 4)$ are the base radii of the four gears, and T_{d1} and T_{d2} denote the dynamic meshing forces of the first- and second-stage gear pairs, respectively.

By selecting the angular displacement and angular velocity of each equivalent inertia disk as state variables, the state-space representation of the system can be established. Subsequently, the torsional vibration response of the system can be solved using the numerical integration solver *Ode15s* in MATLAB. The angular displacements of each equivalent inertia disk, θ_i, are first computed, and the relative torsional angular displacements between adjacent disks are then defined as

$$\theta_{12} = \theta_1 - \theta_2, \theta_{23} = \theta_2 - \theta_3, \theta_{34} = \theta_3 - \theta_4, \theta_{45} = \theta_4 - i_{12} \cdot \theta_5, \theta_{56} = \theta_5 - \theta_6, \theta_{67} = \theta_6 - \theta_7, \theta_{78} = \theta_7 - i_{34} \cdot \theta_8, \tag{6}$$

where i_{12} and i_{34} denote the transmission ratios of the first- and second-stage gear pairs, respectively, defined as $i_{12} = 3$ and $i_{34} = 5$. The physical definitions of the relative torsional angles are listed in Table 3.

To validate the proposed lumped-parameter model, the eigenvalue problem of the undamped free torsional vibration system is solved to obtain its natural frequencies. A corresponding PT–PIC dynamic model is also developed in Romax, and modal analysis is performed to extract the first two torsional natural frequencies and mode shapes. The results show that the relative errors of the first two natural frequencies are both within 2.7 % (see Table 4), confirming that the model accurately captures the system's torsional dynamics and is suitable for subsequent response analysis under torque fluctuation excitation.

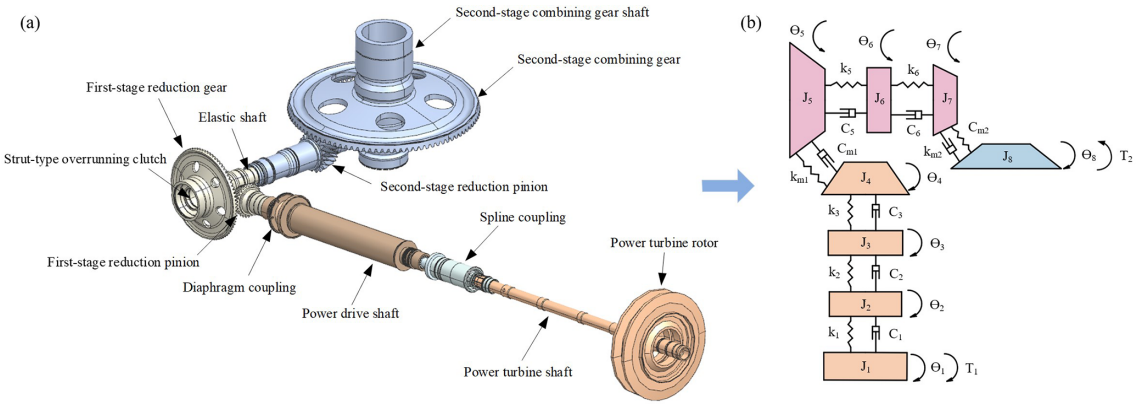

Figure 1. **(a)** Structural configuration of the PT–PIC. **(b)** Dynamic model of the PT–PIC.

Table 1. Rotational inertias of the equivalent disks in the system.

Name	Symbol	Moment of inertia ($\mathrm{kg\,m^2}$)	Name	Symbol	Moment of inertia ($\mathrm{kg\,m^2}$)
Equivalent disk 1	J_1	1.56×10^{-1}	Equivalent disk 5	J_5	3.29×10^{-2}
Equivalent disk 2	J_2	1.22×10^{-3}	Equivalent disk 6	J_6	1.20×10^{-3}
Equivalent disk 3	J_3	2.88×10^{-3}	Equivalent disk 7	J_7	5.22×10^{-3}
Equivalent disk 4	J_4	1.95×10^{-3}	Equivalent disk 8	J_8	8.58×10^{-1}

Because the system belongs to a military helicopter platform, full-scale torsional vibration measurements are not publicly available. In such cases, high-fidelity transmission simulation tools serve as practical engineering benchmarks. The close agreement with Romax therefore provides credible validation, although it is currently limited to modal characteristics rather than response-level experimental data. Future work will incorporate higher-fidelity co-simulation and, when available, experimental measurements to further strengthen validation of torsional vibration responses.

2.3 Engine torque excitation under different operating conditions

Power turbine torque exhibits pronounced nonstationary behavior that varies with flight condition while remaining statistically consistent within each condition. To characterize the excitation, time-domain and statistical analyses are performed using engine data from a representative mission, focusing on three typical operating conditions: hover, aggressive vertical maneuvers, and high-altitude climb and descent maneuver. These scenarios capture distinct rotor power demands and control actions. Hover corresponds to steady hovering or station-keeping flight, during which the engine operates near a quasi-steady state and the rotor power demand remains nearly constant, resulting in small, low-frequency torque fluctuations. Aggressive vertical maneuvers represent rapid low-altitude vertical repositioning (e.g., quick take-off, obstacle avoidance, or emergency climb/descent within $\approx$ 30 m), where frequent collective pitch adjustments generate high-rate, quasi-periodic torque variations and strong transient excitation. In contrast, the high-altitude climb and descent maneuver corresponds to large-altitude transition flight ($\approx$ 200 m), typical of mission transit and terrain clearance, characterized by sustained power increase during climb followed by gradual power reduction during descent, leading to slower but larger-amplitude torque evolution. The corresponding time histories of power turbine torque and speed are presented in Fig. 2, and the fluctuation amplitude ranges are summarized in Table 5.

The analysis shows that torque excitations under different operating conditions differ notably in amplitude, evolution, and local variation rate. First-order statistics, such as amplitude, cannot fully capture the temporal variation characteristics. To quantify these properties, the autocorrelation time τ_c is introduced as a measure of the signal's temporal correlation. A smaller τ_c indicates faster decorrelation and more rapid excitation variations, while a larger τ_c reflects slower evolution.

The autocorrelation time is determined from the normalized autocorrelation function $R(\tau)$, which is defined as follows:

$$R(\tau) = \frac{E\left[\left(T(t) - \overline{T}\right)\left(T(t+\tau) - \overline{T}\right)\right]}{E\left[\left(T(t) - \overline{T}\right)^2\right]}, \tag{7}$$

where $T(t)$ denotes the instantaneous engine torque and $\overline{T}$ its mean value. The autocorrelation time is defined as the time

Table 2. Dynamic parameters of system components.

Component	Parameter	Value	Parameter	Value
Power turbine shaft	k_1 (N m rad^{-1})	7.1×10^3	c_1 (N m s rad^{-1})	3.0×10^{-1}
Spline coupling	k_2 (N m rad^{-1})	1.7×10^5	c_2 (N m s rad^{-1})	2.4×10^{-1}
Diaphragm coupling	k_3 (N m rad^{-1})	1.2×10^6	c_3 (N m s rad^{-1})	3.0×10^{-1}
Strut-type overrunning clutch	k_5 (N m rad^{-1})	7.6×10^3	c_5 (N m s rad^{-1})	3.0×10^1
Elastic shaft	k_6 (N m rad^{-1})	1.5×10^5	c_6 (N m s rad^{-1})	5.2×10^{-1}
Primary transmission gear	k_{m1} (N m^{-1})	5.20×10^8	C_{m1} (N s m^{-1})	1.19×10^2
Secondary transmission gear	k_{m2} (N m^{-1})	9.10×10^8	C_{m2} (N s m^{-1})	7.79×10^2

Table 3. Physical meaning of relative torsional angles.

Description	Symbol	Description	Symbol
Relative torsional angle between the power turbine and the driving part of the spline coupling	θ_{12}	Relative torsional angle of the strut-type overrunning clutch	θ_{56}
Relative torsional angle between the driving and driven parts of the spline coupling	θ_{23}	Relative torsional angle between the two ends of the flexible shaft	θ_{67}
Relative torsional angle between the driven part of the spline coupling and the transmission shaft	θ_{34}	Relative torsional angle of the second-stage gear mesh	θ_{78}
Relative torsional angle of the first-stage gear mesh	θ_{45}	–	–

Table 4. Comparison of torsional natural frequencies obtained from numerical analysis and Romax simulation for the first two system modes.

Mode Order	Mode 1 (Hz)	Mode 2 (Hz)
Numerical Result (Hz)	64.8	146.2
Romax Analysis (Hz)	65.6	142.3
Relative Error (%)	1.2	2.7

lag at which the normalized autocorrelation function decays to $1/e$ of its initial magnitude.

Although the measured torque signals have a relatively low sampling rate (8.3 Hz), resulting in an excitation bandwidth well below the system's natural frequencies, they still exhibit pronounced temporal correlation. Accordingly, the characteristic autocorrelation time τ_c is adopted, instead of the conventional frequency-ratio criterion, to classify excitation.

From a system timescale perspective, torque disturbances typically correspond to periods of 0.01–0.1 s. When $\tau_c < 10$ s, the excitation varies rapidly and is regarded as fast-varying; when $\tau_c > 10$ s, it evolves slowly and approaches quasi-static behavior. Statistical analysis of measured torque data reveals clear separation among operating conditions: $\tau_c > 20$ s for hover, 1020 s for high-altitude climb and descent maneuver, and $\tau_c < 10$ s for aggressive vertical maneuvers.

Based on engine torque data collected from multiple operating conditions during a representative flight mission, statistical analysis reveals a clear separation among conditions: $\tau_c > 20$ s for hover, 1020 s for high-altitude climb and descent maneuver, and $\tau_c < 10$ s for aggressive vertical maneuvers. Integrating theoretical timescale separation, operational characteristics, and statistical evidence, $\tau_c = 10$ and 20 s are selected as classification thresholds. The excitations are therefore categorized as short- ($\tau_c < 10$ s), intermediate- ($10 \le \tau_c \le 20$ s), and long-correlation time ($\tau_c > 20$ s). Table 6 shows strong agreement with the statistical distributions, confirming the effectiveness of this classification for characterizing torque variation rates and supporting subsequent PIC torsional response analysis.

Combined with the analysis in Sect. 2.1, the autocorrelation time τ_c is found to characterize the time-domain variation rate of torque and is intrinsically related to the ramp excitation parameter α. Specifically, a smaller τ_c corresponds to a larger α, which is more likely to induce pronounced transient torsional responses. This provides a theoretical basis for subsequent comparisons of PIC responses under different operating conditions.

3 Influence of engine torque fluctuations on the torsional vibration response of the PIC

Based on the coupled PT–PIC dynamic model, this section evaluates the effects of engine torque fluctuations on torsional vibration under different flight conditions. Measured

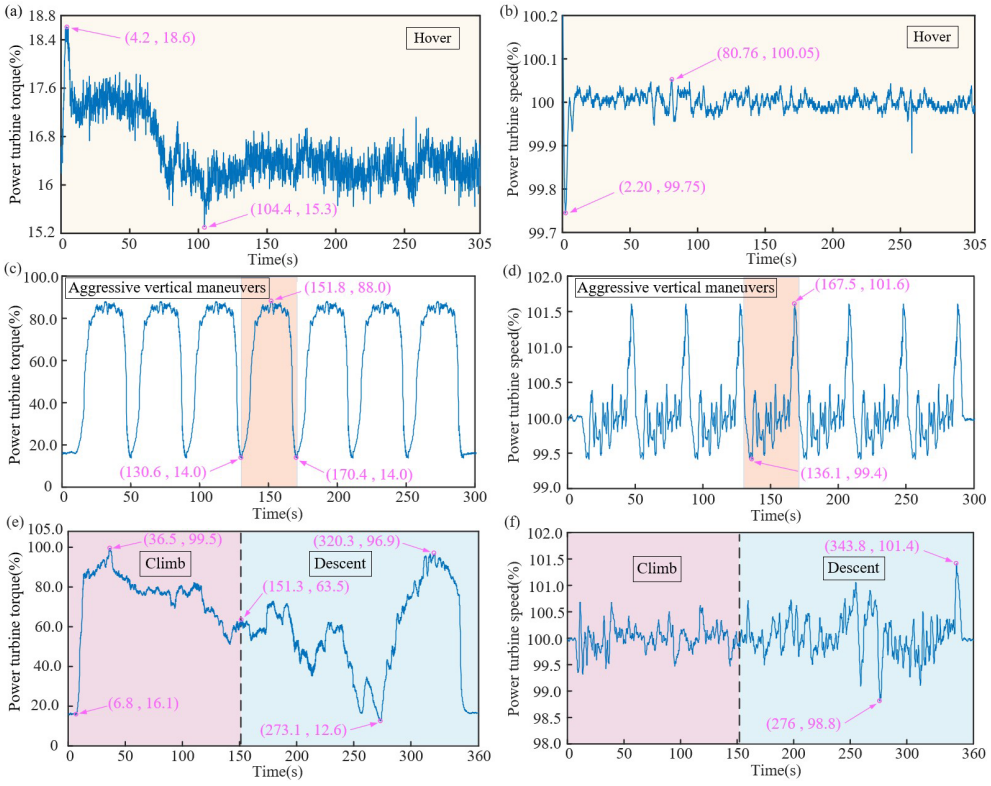

Figure 2. Power turbine torque (left column) and speed (right column) under three representative flight conditions: **(a–b)** hover, **(c–d)** aggressive vertical maneuvers, and **(e–f)** high-altitude climb and descent maneuver.

Table 5. Time-domain characteristics of engine torque excitations under three representative flight conditions.

Operating condition amplitude	Torque fluctuation (% of maximum torque)
Hover	15.3 %–18.6 %
High-altitude climb and descent maneuver	12.6 %–96.9 %
Aggressive vertical maneuvers	14.0%–88.0%

torque signals from three representative conditions are applied as excitation inputs, the system equations are solved numerically to obtain key node responses, and the underlying mechanisms are interpreted from the perspective of excitation temporal characteristics.

3.1 Torsional vibration response characteristics of the PIC under different operating conditions

To investigate how engine torque fluctuations affect the torsional vibration of the PIC, measured torque excitations under three typical flight conditions were applied as inputs. Based on the autocorrelation time τ_c, hover, high-altitude climb and descent maneuver, and aggressive vertical maneuvers are classified as slow-, moderate-, and fast-varying excitations, respectively. The lumped-parameter method is then used to compute and compare the system's torsional responses.

Representative nodes were selected to capture the coupling between torque fluctuations and system response, including the relative angle between the turbine-disk equivalent inertia and spline coupling driving end (θ_{12}), across the strut-type overrunning clutch (θ_{56}), and the mesh-level relative torsional angles of the two gear stages (θ_{45} and θ_{78}). Under the high-altitude climb and descent maneuver (Fig. 3), a clear hierarchical distribution of response amplitudes is observed: θ_{56} is the largest (5.512×10^{-2} rad), followed by θ_{12} (2.025×10^{-2} rad), whereas θ_{78} is the smallest (3.013×10^{-7} rad). The same trend appears in the other conditions. This disparity arises from drivetrain inertia and stiffness distributions. Components near the excitation source (turbine, spline coupling) have high equivalent inertia and low torsional stiffness, enabling large angular deformation

Table 6. Autocorrelation time τ_c and classification of torque variation rates under three representative flight conditions.

Flight condition	Hover	High-altitude climb and descent maneuver	Aggressive vertical maneuvers
Torque autocorrelation time τ_c (s)	24.0	13.3	6.4
Excitation variation rate	Slow	Intermediate	Fast

and transient energy accumulation. Conversely, gear meshes possess very high meshing stiffness and strong kinematic constraints, limiting relative deformation along the line of action; torsional energy is transmitted as torque rather than stored elastically. Consequently, mesh-level angles are orders of magnitude smaller than clutch-level angles, identifying the clutch and spline coupling as primary torsional compliance sites and the gear stages as high-stiffness transmission paths.

For brevity, only the response under aggressive vertical maneuvers is additionally shown (Fig. 4). Across the three conditions, increasing temporal variability of the torque excitation (i.e., decreasing τ_c and increasing variation rate) leads to substantial growth in both response amplitude and fluctuation range. Under aggressive vertical maneuvers, the amplitude of θ_{56} reaches 6.083×10^{-2} rad, which is 10.3 % higher than that under the high-altitude climb and descent maneuver (5.512×10^{-2} rad) and 280.0 % higher than that under hover (1.599×10^{-2} rad). This indicates that rapid torque variations enhance internal energy coupling and produce pronounced dynamic amplification in the PIC torsional response.

Analysis of peak responses under aggressive vertical maneuvers shows that maximum torsional vibrations do not coincide with torque peaks and are not directly correlated with torque amplitude. Instead, the vibration intensity is primarily governed by the temporal variation of the excitation. This is confirmed by the first-order time derivatives of turbine torque and rotational speed (Fig. 5), whose peaks align with those of θ_{12} and θ_{56}, indicating that strong transient responses arise from rapid torque changes rather than absolute magnitude.

Overall, the temporal correlation of engine torque fluctuations, quantified by the autocorrelation time τ_c, is the dominant factor controlling torsional vibration intensity. As τ_c decreases, both response amplitudes and transient peaks increase, particularly at critical components such as the strut-type overrunning clutch and spline coupling. These results demonstrate that the high variation rate of torque excitations amplifies system torsional vibrations and that rapid torque fluctuations under typical operating conditions are the primary cause of intensified responses.

3.2 Comparative analysis of torsional vibration responses under different operating conditions

To investigate the differences in torsional responses under typical operating conditions and the effects of distinct excitation characteristics, a comparative analysis is conducted for three representative flight conditions. Response amplitudes and peak-to-peak values at each node are extracted, and their distributions are shown in Fig. 6. The results indicate that, except for gear pair nodes, most nodes exhibit the largest relative torsional displacement amplitudes under aggressive vertical maneuvers due to stronger excitation from rapid torque fluctuations. In contrast, the hover condition shows the smallest amplitudes, indicating better vibration stability. Among all nodes, θ_{12} and θ_{56} consistently exhibit the largest fluctuations, significantly exceeding those of the secondary gear pair θ_{78}, suggesting that disturbances originate near the power turbine–coupling region and attenuate along the transmission path. This behavior is governed by the system's inertia distribution and torsional stiffness matching. Furthermore, differences in torque variation rates across operating conditions influence not only the response magnitude but also the dynamic coupling and spatial distribution of vibration amplitudes within the system.

To examine the relationship between system response and excitation characteristics, the torque values at the instant when θ_{56} reaches its maximum are extracted and compared with the corresponding fluctuation ranges. Under hover, high-altitude climb and descent maneuver, and aggressive vertical maneuvers, these values are 16.2 %, 68.6 %, and 57.8 % of the maximum torque, respectively, none coinciding with the torque peaks. Combined with node response comparisons, this indicates that torsional vibration intensity does not scale linearly with torque amplitude, and the fluctuation range alone is insufficient to predict system responses.

To further clarify the mechanism, the first derivative of the torque signals is computed, and the variation-rate curves are shown in Fig. 7. The aggressive vertical maneuver condition exhibits the largest variation rate, followed by high-altitude climb and descent maneuver, while hover shows the smallest, consistent with the distribution of response amplitudes. This confirms that torsional vibration intensity is primarily governed by the torque variation rate rather than its amplitude. Mechanistically, a high variation rate prevents instantaneous inertial equilibrium, leading to transient energy accumulation and dynamic amplification. Overall, response amplitudes are determined by inertia and stiffness distribution, while higher torque variation rates increase vibration intensity and dynamic loads. Rapid torque fluctuations can significantly amplify relative torsional displacements in critical components, such as the strut-type overrunning clutch and

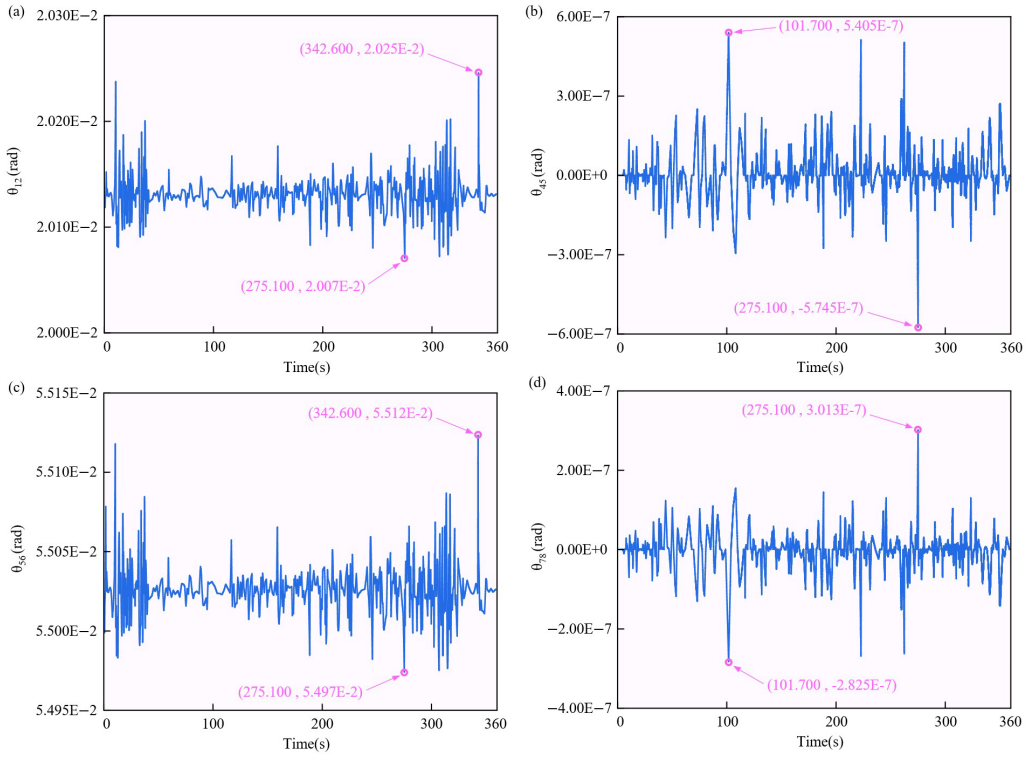

Figure 3. Torsional angle responses of the system under the high-altitude climb and descent maneuver: **(a)** θ_{12}, **(b)** θ_{45}, **(c)** θ_{56}, and **(d)** θ_{78}.

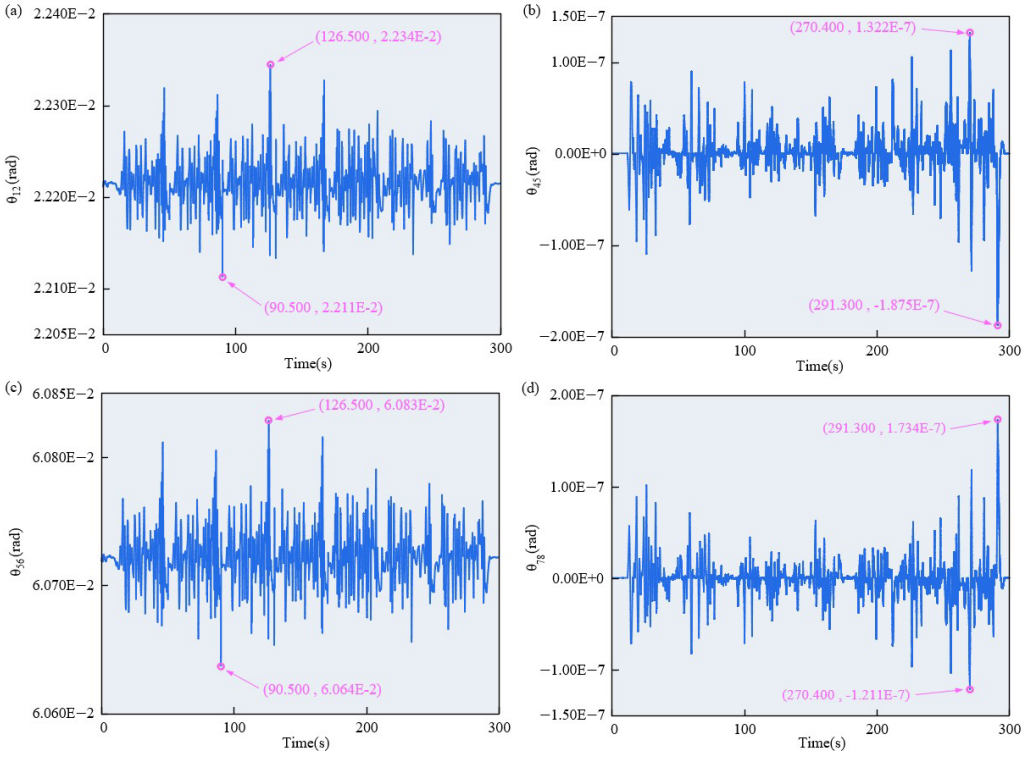

Figure 4. Torsional angle responses of the system under the aggressive vertical maneuvers: **(a)** θ_{12}, **(b)** θ_{45}, **(c)** θ_{56}, and **(d)** θ_{78}.

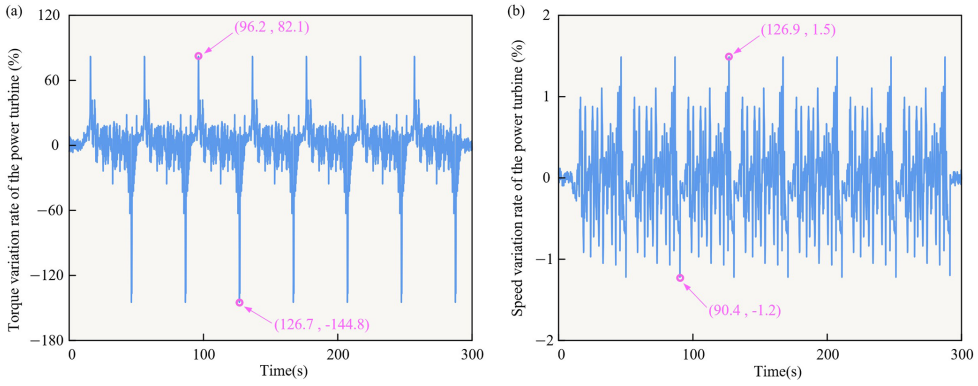

Figure 5. Characteristics of the power turbine under aggressive vertical maneuvers: **(a)** torque variation rate and **(b)** speed variation rate.

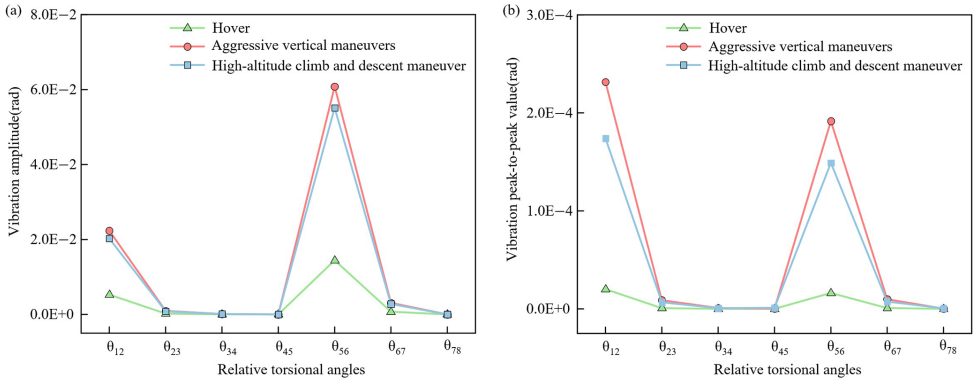

Figure 6. Comparison of torsional responses under three flight conditions: **(a)** amplitudes and **(b)** peak-to-peak values.

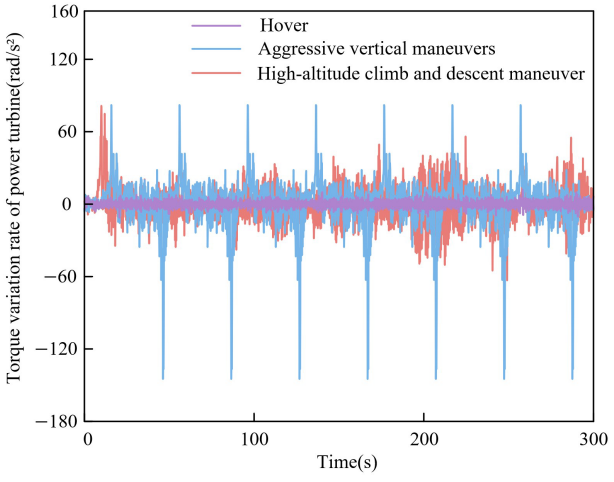

Figure 7. Comparison of power turbine torque variation rates under three representative flight conditions.

spline coupling, thereby increasing the risk of fatigue and failure.

In summary, comparative analysis under three representative operating conditions confirms that the time-varying characteristics of torque excitation dominate the system's torsional vibration behavior. The torque variation rate is identified as the key parameter governing the dynamic response, with a significantly greater influence than other excitation features. Therefore, in the dynamic design and control of the PIC, special attention should be given to the effects of high-rate torque excitation on system stability and fatigue reliability.

4 Conclusions

This study investigates the effects of engine torque fluctuations on the torsional vibration responses of the PT–PIC system under typical flight conditions. A lumped-parameter dynamic model is established, and, combined with measured torque data, the response characteristics and underlying mechanisms are systematically analyzed. The main conclusions are as follows:

1. Comparative analysis under three representative conditions shows that the strut-type overrunning clutch location (θ_{56}) consistently exhibits the largest torsional vibration amplitude, identifying it as the most sensitive region and a potential weak point for fatigue failure. This highlights the need for careful stiffness matching and fatigue-resistant design at this location.

2. The torque variation rate primarily governs the torsional vibration intensity. As the rate increases, the transient response is significantly amplified. Across the hover, high-altitude climb and descent maneuver, and aggressive vertical maneuver conditions, the variation rate increases sequentially, and the vibration amplitude at θ_{56} shows a clear rising trend by approximately 10.3 % relative to the high-altitude climb and descent maneuver and 280.0 % relative to hover. These results demonstrate that the high variation rate of torque excitation dominates the system response, with a much greater influence than the torque amplitude.

3. The study establishes the intrinsic relationship between torque fluctuation characteristics and torsional responses of the PIC, providing a theoretical basis for vibration mechanism analysis, fatigue assessment, and structural optimization. Future work will incorporate parameter sensitivity analysis and key nonlinear effects, such as oil film dynamics, to improve model accuracy under complex conditions.

Data availability. Data will be made available on request.

Author contributions. Hongli Yue: investigation, software, data curation, writing – original draft, formal analysis. Chao Li: investigation, software, formal analysis. Guangfu Bin: conceptualization, methodology, writing – review and editing, project administration, supervision. Xianghuan Liu: conceptualization, methodology, investigation. Jian Li: conceptualization, methodology, investigation. Anhua Chen: conceptualization, methodology, investigation. Qiang Li: conceptualization, methodology, investigation.

Competing interests. The contact author has declared that none of the authors has any competing interests.

Disclaimer. Publisher's note: Copernicus Publications remains neutral with regard to jurisdictional claims made in the text, published maps, institutional affiliations, or any other geographical representation in this paper. The authors bear the ultimate responsibility for providing appropriate place names. Views expressed in the text are those of the authors and do not necessarily reflect the views of the publisher.

Acknowledgements. This work was supported by the National Natural Science Foundation of China (grant nos. 12572061, 52405103), the Hunan Provincial Natural Science Foundation Project (grant nos. 2024JJ6216, 2024JJ5156), the 77th Batch of General Projects of the China Postdoctoral Science Foundation (grant no. 2025M771339), and the Science and Technology Innovation Program of Hunan Province (grant no. 2025RC4015).

Financial support. This research was supported by the National Natural Science Foundation of China (grant nos. 12572061, 52405103), the Hunan Provincial Natural Science Foundation Project (grant nos. 2024JJ6216, 2024JJ5156), the 77th Batch of General Projects of the China Postdoctoral Science Foundation (grant no. 2025M771339), and the Science and Technology Innovation Program of Hunan Province (grant no. 2025RC4015)

Review statement. This paper was edited by Hui Ma and reviewed by three anonymous referees.

References

Che, X., Yu, H., Zhang, C., and Sun, Z.: Effect of floating spline parameters on dynamic characteristics of an encased differential planetary gear train, Sci. Rep., 14, 8349, https://doi.org/10.1038/s41598-024-59094-4, 2024.

Chi, C., Yan, X., Chen, R., and Li, Y.: Analysis of low-speed height-velocity diagram of a variable-speed-rotor helicopter in one-engine-failure, Aerosp. Sci. Technol., 91, 310–320, https://doi.org/10.1016/j.ast.2019.05.003, 2019.

Davies, D. P., Jenkins, S. L., and Belben, F. R.: Survey of fatigue failures in helicopter components and lessons learned, Eng. Fail. Anal., 32, 134–151, https://doi.org/10.1016/j.engfailanal.2013.03.005, 2013.

de Voogt, A. and St Amour, E.: Safety of twin-engine helicopters: Risks and operational specificity, Saf. Sci., 136, 105169, https://doi.org/10.1016/j.ssci.2021.105169, 2021.

Han, H., Lee, K., and Park, S.: Fatigue life estimation of propulsion shafts from torsional vibration measurements using linear damage summation, Ocean Eng., 107, 212–221, https://doi.org/10.1016/j.oceaneng.2015.07.023, 2015.

Hu, J., Hu, N., Yang, Y., and Chen, M.: Nonlinear dynamic modeling of a helicopter planetary gear set for tooth crack diagnosis, Measurement, 198, 111347, https://doi.org/10.1016/j.measurement.2022.111347, 2022.

Hu, J., Yang, Y., Hu, N., and Chen, M.: Dynamic modeling and characteristic analysis of a helicopter main reducer for tooth crack diagnosis, Measurement, 2025, 116823, https://doi.org/10.1016/j.measurement.2025.116823, 2025.

Li, Z., Ma, Y., Wei, Z., and Sun, Q.: Structured neural-network-based modeling of hybrid-electric turboshaft engine startup process, Aerosp. Sci. Technol., 128, 107740, https://doi.org/10.1016/j.ast.2022.107740, 2022.

Lin, H., Yu, Q., and He, G.: Vibration analysis of thin-walled bearing in harmonic reducer under periodic loading, J. Sound Vib., 614, 119174, https://doi.org/10.1016/j.jsv.2025.119174, 2025.

Liu, Z., Huangfu, Y., Ma, H., and Li, X.: Traveling-wave resonance analysis of flexible spur gear systems with angular misalignment, Int. J. Mech. Sci., 232, 107617, https://doi.org/10.1016/j.ijmecsci.2022.107617, 2022.

Ma, J., Liu, G., Li, J., and Zhang, Y.: Evaluation of energy-saving potential of an aero-engine pre-swirl system, Appl. Energy, 359, 122601, https://doi.org/10.1016/j.apenergy.2023.122601, 2024.

Mo, S., Huang, X., Liu, W., and Zhao, M.: Nonlinear vibration and primary resonance of helicopter face-gear planetary trans-

mission system, Proc. Inst. Mech. Eng. Part K, 237, 534–554, https://doi.org/10.1177/14644193231188776, 2023.

Shen, Z., Qiao, B., Yang, L., and Liu, H.: Fault mechanism and dynamic modeling of planetary gears with gear wear, Mech. Mach. Theory, 155, 104098, https://doi.org/10.1016/j.mechmachtheory.2020.104098, 2021.

Sheng, H., Chen, Q., Li, J., and Wang, Y.: Dynamic modeling and performance analysis of helicopter turboshaft engine startup, Aerosp. Sci. Technol., 106, 106097, https://doi.org/10.1016/j.ast.2020.106097, 2020.

Song, J., Chen, Y., Li, W., and Zhang, H.: Nonlinear model predictive control for high-speed helicopter power systems, Aerosp. Sci. Technol., 2025, 110093, https://doi.org/10.1016/j.ast.2025.110093, 2025.

van Binsbergen, D., Valavi, M., Nejad, A. R., and Zimroz, R.: Generator torque ripple optimization and its influence on geared drivetrain dynamics, Forsch. Ingenieurwes., 87, 197–205, https://doi.org/10.1007/s10010-023-00624-3, 2023.

Vladov, S., Bulakh, M., Baranovskyi, D., and Hrytsenko, O.: Neural-network-based combustion chamber monitoring for helicopter turboshaft engines, Measurement, 242, 116267, https://doi.org/10.1016/j.measurement.2024.116267, 2025.

Wang, X. and Xia, P.: Modeling and vibration analysis of helicopter drivetrain systems, AIAA J., 60, 4288–4301, https://doi.org/10.2514/1.J061493, 2022.

Yang, X., Ding, K., He, G., and Wang, Y.: AM–FM sideband vibration modeling of planetary gear sets with distributed faults, Mech. Mach. Theory, 179, 105093, https://doi.org/10.1016/j.mechmachtheory.2022.105093, 2023.

Zhu, H., Hu, S., Zhang, L., and Zhao, Y.: Dynamic characteristics of a supercritical helicopter tail transmission system with rubbing impact, Int. J. Struct. Stab. Dyn., 24, 2450188, https://doi.org/10.1142/S0219455424501888, 2024.